

1 **Time-resolved analyses of elemental distribution and concentration in living plants: An example**
2 **using manganese toxicity in cowpea leaves**

3
4 F. Pax C. Blamey¹, David J. Paterson², Adam Walsh², Nader Afshar², Brigid A. McKenna¹, Miaomiao
5 Cheng³, Caixian Tang³, Walter J. Horst⁴, Neal W. Menzies¹, and Peter M. Kopittke^{1*}

6
7 ¹The University of Queensland, School of Agriculture and Food Sciences, St. Lucia, Queensland
8 4072, Australia; ²Australian Synchrotron ANSTO, Clayton, Victoria 3168, Australia; ³La Trobe
9 University, Centre for AgriBioscience, Bundoora, Victoria 3086, Australia; ⁴Leibniz University,
10 Institute of Plant Nutrition, Hannover, Germany.

11
12
13 Author for correspondence:

14 *Peter M. Kopittke*

15 *Tel: +61 7 3346 9149*

16 *Email: p.kopittke@uq.edu.au*

17
18 **Word count:**

19 **Summary:** 191

20 **Introduction:** 931

21 **Materials and Methods:** 1902

22 **Results:** 1356

23 **Discussion:** 1140

24 **Conclusion:** 181

25 **Acknowledgements:** 68

26 **Total word count (above sections): 5769**

27
28 **Number of figures:** 6 (plus 3 in Supporting Information)

29 **Figures in color:** 1, 2, 3, 4, 5, (plus 3 in Supporting Information)

30 **Number of tables:** 0 (plus 1 in Supporting Information)

31

32

33

34 **Summary**

35

36 • Knowledge of elemental distribution and concentration within plant tissues is crucial in the
37 understanding of almost every process that occurs within plants. However, analytical
38 limitations have hindered the microscopic determination of changes over time in the location
39 and concentration of nutrients and contaminants in living plant tissues.

40 • We developed a novel method using synchrotron-based micro X-ray fluorescence (μ -XRF)
41 that allows for laterally-resolved, multi-element, kinetic analyses of plant leaf tissues *in vivo*.
42 To test the utility of this approach, we examined changes in the accumulation of Mn in
43 unifoliate leaves of 7-d-old cowpea (*Vigna unguiculata*) plants grown for 48 h at 0.2 and 30
44 μ M Mn in solution.

45 • Repeated μ -XRF scanning did not damage leaf tissues demonstrating the validity of the
46 method. Exposure to 30 μ M Mn for 48 h increased the initial number of small spots of
47 localized high Mn and their concentration rose from 40 to 670 mg Mn kg⁻¹ fresh mass.
48 Extension of the two-dimensional μ -XRF scans to a three-dimensional geometry provided
49 further assessment of Mn localization and concentration.

50 • This method shows the value of synchrotron-based μ -XRF analyses for time-resolved *in vivo*
51 analysis of elemental dynamics in plant sciences.

52

53 **Key words:** cowpea, ionomics, manganese, micro X-ray fluorescence, synchrotron

54

55

56 **Introduction**

57

58 The concentration and distribution of nutrients and contaminants within plant tissues change over time
59 in response to physiological stimuli, developmental stage, and changes in the broader external
60 environment. To understand the underlying genetic and physiological processes influencing plant
61 growth, it is necessary to determine the concomitant changes in the accumulation or decline of these
62 elements within plant tissues. In this regard, ionomics is concerned with the examination of elements
63 in plants, although measurements are normally conducted for bulk tissues (Salt *et al.*, 2008). Whilst
64 such analyses provide valuable information, it is even more useful to determine laterally resolved
65 concentrations of essential and non-essential elements within plant tissues (Conn & Gilliam, 2010).
66 Besides its relevance in plant nutrition, ionomics involves the functional analysis of genes that
67 directly and indirectly control plant development and physiology (Salt *et al.*, 2008; Takahashi *et al.*,
68 2009).

69 Various techniques exist for examining the distribution of elements within plant tissues but
70 most techniques require extensive processing of sequential samples. Hence, they are not able to
71 examine nutrient and contaminant changes over time in the same area of living plants. For example,
72 conventional scanning electron microscopy coupled with energy-dispersive X-ray spectroscopy
73 (SEM-EDS) needs an ultra-high vacuum that requires samples to be dehydrated; frozen samples may
74 be used where a cryo-SEM-EDS is available (Cosio *et al.*, 2005). It is perhaps possible to examine
75 living plants using environmental SEM (ESEM), but there are problems with sample size restrictions,
76 electron beam damage, and a comparatively poor detection limit (Danilatos, 1981; McGregor &
77 Donald, 2010). Though having excellent subcellular resolution, nanoscale secondary ion mass
78 spectrometry (NanoSIMS) analysis also requires ultra-high vacuum (Moore *et al.*, 2014). Confocal
79 microscopy with fluorophores is potentially of use for the kinetic analyses of living plants (Walczysko
80 *et al.*, 2000; Babourina & Rengel, 2009) but there are limits imposed by the availability of
81 fluorophores and uncertainty in their selectivity and cellular penetration. Laser ablation inductively
82 coupled plasma mass spectrometry (LA-ICP-MS) is also capable of examining living plants in
83 ambient conditions (Salt *et al.*, 2008) but damage through ablation of the sample surface prevents
84 kinetic analysis of the same tissue area. Autoradiography has been used for the study of plants since
85 the 1920s (Hevesy, 1923), and macro-autoradiography can potentially be used for kinetic analyses of
86 living plants but is limited by poor resolution, long exposure times, limited availability of suitable
87 isotopes, and safety considerations (Solon *et al.*, 2010). Recently-developed radioisotope tracer
88 techniques for *in vitro* analysis, such as a positron-emitting tracer imaging system (Tsukamoto *et al.*,
89 2006) and magnetic resonance imaging (Jahnke *et al.*, 2009), have overcome some limitations, but it
90 is only possible to examine a single element at a time (Sugita *et al.*, 2016).

91 Synchrotron-based micro-X-ray fluorescence spectroscopy (μ -XRF) is of interest as there are
92 no theoretical restrictions on sample size, analyses are conducted at ambient temperature and pressure

93 often at a resolution of $c. \leq 1 \mu\text{m}$ with a detection limit of $c. 0.1$ to 100 mg kg^{-1} fresh mass (FM). Leaf
94 tissues of living plants may be examined also (Scheckel *et al.*, 2004). Depending upon the element of
95 interest and beamline specifications, this technique can simultaneously generate maps for multiple
96 elements within the energy range of the beamline, often 2 to 25 keV allowing analysis from P to Ag at
97 the K-edge. Early analyses of plant tissues using μ -XRF analyses focused on dehydrated tissues of
98 hyperaccumulators (McNear *et al.*, 2005; McNear & Küpper, 2014). However, tissue dehydration
99 may result in experimental artifacts and the high concentrations used in studies of hyperaccumulators
100 are not relevant to many crop species. With progressive improvements in technology (specifically, the
101 development of more efficient fluorescent X-ray detectors), there has been increasing interest in the
102 analysis of hydrated tissues of non-hyperaccumulating species (Lombi *et al.*, 2011a; Blamey *et al.*,
103 2015; Kopittke *et al.*, 2015). For example, studies of Cu, Ni, Zn, and Mn rhizotoxicity in hydrated
104 cowpea (*Vigna unguiculata*) roots showed Cu located in the rhizodermis and outer cortex, Ni in the
105 inner cortex, and Zn in the stele; the meristematic zone was high in both Zn and Mn (Kopittke *et al.*,
106 2011; Kopittke *et al.*, 2013). However, problems may still arise with radiation damage and leaf tissue
107 dehydration by high-energy X-rays upon repeated scanning of the same area of leaf (Lombi & Susini,
108 2009) that would preclude repeated analysis of living tissues.

109 To examine the potential of synchrotron-based μ -XRF for the analysis of living plants, we
110 inspected changes in element distribution in leaves of cowpea following exposure to an adequate and
111 a toxic level of Mn in the rooting medium. Using μ -XRF, we previously identified high Mn in
112 sunflower (*Helianthus annuus*) trichomes and in vacuoles of white lupin (*Lupinus albus*) as
113 mechanisms of tolerance (Blamey *et al.*, 2015). Such mechanisms are not present in cowpea (an
114 established model species in Mn toxicity studies) and soybean (*Glycine max*), making these crop
115 species considerably more sensitive to high Mn^{2+} in the root environment that results from the
116 localized accumulation of Mn in leaf tissues (Heenan & Carter, 1976; Horst, 1983). The first visible
117 symptom of toxicity is the appearance of small dark spots on unifoliate leaves $c. 4$ -d after exposure of
118 roots to $20 \mu\text{M}$ Mn (Wissemeier & Horst, 1987). Thus, the present study tested the suitability of μ -
119 XRF for *in situ*, multi-element, kinetic, microscopic analyses to quantify changes in elemental
120 distribution in leaves of living cowpea plants. We envisage that the method developed here will be of
121 importance across a wide range of studies for the examination of plant responses to physiological
122 stimuli, developmental stage, and changes in biotic and abiotic environments.

123

124 **Materials and Methods**

125

126 **Plant growth**

127

128 Cowpea (*Vigna unguiculata* L. Walp. cv. Bunya) seeds in rolled paper towels were placed in tap
129 water and seedlings transplanted 4 d later into 20 L of aerated nutrient solution at pH 5.6 and ionic

130 strength of *c.* 3 mM (Blamey *et al.*, 2015) approximating that in soil solutions (Kopittke *et al.*, 2010).
131 Nominal concentrations of nutrients in the basal solution were (μM): 1000 Ca, 120 $\text{NH}_4^+\text{-N}$, 95 Mg,
132 300 K, 10 Na, 6 Fe, 0.2 Mn, 0.5 Zn, 0.2 Cu, 1250 Cl, 670 $\text{NO}_3^-\text{-N}$, 340 S, 5 P, 1 B, and 0.01 Mo.
133 After 7 d in a controlled environment room at 25 °C under fluorescent lights, plants were transferred
134 to the Australian Synchrotron and grown in fresh nutrient solutions at 22 °C under high-pressure
135 sodium lights at photosynthetically active radiation (PAR) of 1,500 $\mu\text{mol m}^{-2} \text{s}^{-1}$. Mean
136 concentrations of selected nutrients measured by inductively coupled optical emission spectroscopy
137 (ICP-OES) in solutions at the beginning and end of the initial and final periods were (μM): 1,050 Ca,
138 120 Mg, 360 K, 30 Na, 0.23 Mn, 10 Fe, 0.4 Zn, 0.2 Cu, 360 S, 7 P, and 4 B. Use of 15 % $\text{NH}_4^+\text{-N}$ in
139 solution ensured that the initial solution pH 5.6 did not require adjustment.

140 A preliminary experiment tested if repeated $\mu\text{-XRF}$ scans (see below) of the same area of leaf
141 caused damage that would potentially modify the transport of solutes in the xylem and phloem or
142 cause other experimental artifacts (e.g. dehydration). This involved excision of a unifoliate leaf
143 followed by mounting between two layers of 4- μm Ultralene[®] film on a specimen holder that
144 provided support and limited dehydration (Fig. 1a).

145 The main experiment involved the transfer of four plants, each to a 50-mL polypropylene
146 centrifuge tube (30 × 115 mm) with roots submerged in 40 mL of basal nutrient solution. Securing the
147 plant stem in the neck of the tube by rolling a length of 15-mm wide geotextile covered by a slotted
148 cap and Parafilm M[®] prevented spillage onto sensitive equipment. Also secured in the neck of the
149 centrifuge tube were two 2-m lengths of PTFE #2 AWG thin-wall tubing (Cole-Parmer Instrument
150 Company, Vernon Hills IL, USA), one serving as solution input and the other as output. Tygon[®]
151 tubing with 0.7-mm internal diameter joined the PTFE tubing where necessary. The input tube
152 connected a 10-L reservoir of continuously aerated nutrient solution via a four-roller peristaltic pump
153 to the bottom of the solution in the centrifuge tube. The output tube extended from the 40-mL mark of
154 the centrifuge tube to the reservoir via the peristaltic pump, adjustment of which ensured no solution
155 overspill. Circulation of nutrient solution between the reservoir and the centrifuge tube at a measured
156 rate of 4 mL min^{-1} enabled 90 % renewal of the 40 mL of nutrient solution in < 30 min. Two purpose-
157 built sample holders, each with two centrifuge tubes, contained plants fixed to each holder. Securing a
158 unifoliate leaf of each plant with Ultralene[®] and double-sided tape protected the sensitive Be detector
159 window *c.* 1 mm away but also allowed transpiration via both the adaxial and abaxial leaf surfaces
160 (Fig. 2a). Each sample holder (i.e. replicate) with two secured plants was attached in turn to the
161 sample stage that allowed horizontal and vertical adjustment of the leaves and correct focusing of the
162 X-ray beam (Fig. 2b). With solution in each centrifuge tube connected to a 10 L-reservoir, we
163 imposed two treatments with nominal 0.2 (i.e. basal) and 30 μM Mn. Mean measured values at the
164 start and end of the 48-h experimental period were 0.33 and 30 μM Mn.

165 An important objective of the main experiment was ensuring optimal plant growth conditions
166 other than in the 30 μM Mn treatment. We had initially intended to renew the 40 mL of solution in

167 each centrifuge tube at appropriate intervals, but an anticipated rapid decrease in dissolved O₂
168 precluded this approach. Specifically, we calculated that a 7-d-old root system (2.5 g FM plant⁻¹) with
169 an O₂ consumption rate of 20 μmol g⁻¹ FM h⁻¹ (Bravo & Uribe, 1981) would deplete the 510 μmol
170 dissolved O₂ in 40 mL solution at 25 °C in < 30 min. Thus, root O₂ and nutrient requirements over 48
171 h were met by circulating 10 L of aerated solution. Use of a peristaltic pump and reservoirs placed on
172 the floor proved satisfactory provided the outflow rate exceeded that of the inflow to prevent overflow
173 of the 50-mL centrifuge tube. This ensured the safety of sensitive electronic equipment that had
174 previously been avoided through use of solid growth medium (Scheckel *et al.*, 2004) or a small
175 reservoir of solution with *Arabidopsis thaliana* plants (Fittschen *et al.*, 2017). Additionally, we had to
176 prevent damage to the fragile Be window of the Maia detector despite the need for unifoliate leaves
177 being at a distance of *c.* 1 mm for correct focus ([http://www.synchrotron.org.au/aussyncbeamlines/x-](http://www.synchrotron.org.au/aussyncbeamlines/x-ray-fluorescence-microscopy/samples)
178 [ray-fluorescence-microscopy/samples](http://www.synchrotron.org.au/aussyncbeamlines/x-ray-fluorescence-microscopy/samples)). Securing the unifoliate leaves to the sample holder with
179 Ultralene[®] and double-sided tape (Fig. 2a) and moving the other leaves away from the detector (Fig. 2
180 b) overcame this potential problem.

181 The final experiment of this study determined the bulk concentration of Mn in unifoliate
182 leaves of cowpea plants grown in a laboratory under high-pressure sodium lights at 25 °C using the
183 same procedure as above. Four plants in each of six 20-L pots were grown in basal nutrient solution
184 for 7 d after transplanting at which time three replicates of 0.2 and 30 μM Mn were imposed for 2 d.
185 Mean concentrations of selected nutrients in solution measured by ICP-OES were (μM): 820 Ca, 85
186 Mg, 50 K, 20 Na, 10 Fe, 0.28 Zn, 0.12 Cu, 150 S, 10 P, and 2.7 B. The mean concentration of Mn was
187 0.23 and 28 μM in the two treatments at the start and end of 2 d. Four unifoliate leaves were harvested
188 from each pot, FM and dry mass (DM) determined, and leaves digested in 5:1 HNO₃:HClO₄ prior to
189 Mn analysis using ICP-OES.

190

191 **μ-XRF scans**

192

193 Details of the XFM beamline at the Australian Synchrotron have been provided by Paterson
194 *et al.* (2011), as have details for the analysis of fresh hydrated roots by Kopittke *et al.* (2011) and
195 leaves by Blamey *et al.* (2015). X-rays, at an energy of 12.9 keV in the present study, were selected
196 using a Si(111) monochromator and focused (2 × 2 μm) by a pair of Kirkpatrick-Baez mirrors and the
197 X-ray fluorescence emitted by the specimen collected in a backscatter geometry using a 384-element
198 Maia detector system (Lombi *et al.*, 2011a; Paterson *et al.*, 2011). Elemental mapping is conducted
199 on-the-fly in the horizontal direction. Until recently, discrete steps in the vertical direction increased
200 the dwell at the edge of the scanned area (i.e. at the end of each horizontal line scan) with greater
201 potential for X-ray damage to hydrated tissues. A recent improvement allows significantly faster and
202 more accurate raster scanning via kinematically optimized fly-scans known as Rascan, a system that
203 wraps the motion controller into an optimal two-dimension scanner. This device renders a motion

204 trajectory optimized for smoothness, as well as minimal overhead times, for a given fly-scan of
205 known transit time (dwell) and pitch. Importantly, Rascan reduces end-of-line overheads from > 350
206 ms to *c.* 35 ms resulting in a *c.* 30 % reduction in scan time and less radiation damage. Using this
207 approach, analyses are routinely conducted with a dwell of ≤ 1 ms pixel⁻¹, comparing favorably to
208 many other synchrotron-based μ -XRF beamlines where a dwell of 10 to 100 ms pixel⁻¹ is common
209 (Lombi *et al.*, 2011b). This decreased dwell using the Maia detector system and Rascan at the
210 Australian Synchrotron facilitated the present study with repeated scanning of the same area of living
211 plant leaf tissues.

212 The preliminary experiment determined if sequential scanning of the same area resulted in
213 damage from high energy X-rays. The survey scan started within 5 min of excising and mounting a
214 unifoliate leaf (Fig. 1a) and took 52 min to complete an area of 47×33 mm with a step size (i.e.
215 virtual pixel size) of 50 μ m. From this survey scan, a 7×3 mm area was selected for further
216 examination with three detailed scans with a step size of 5 μ m, each scan taking *c.* 20 min. Each of
217 the detailed scans covered a slightly larger area encompassing the entire previous scan to test if the X-
218 rays damaged the leaf that would be evident in the subsequent scans by changes in sample hydration
219 and elemental redistribution. A fourth, high-resolution scan with a step size of 2 μ m covering an area
220 of 1.54×0.79 mm tested the possibility of damage in detail. We also used light microscopy to
221 examine the leaf for any visible signs of damage.

222 Thereafter, the main experiment involved securing the sample holder with two centrifuge
223 tubes, each with a living plant (Fig. 2), in the beamline and verifying basal solution (0.2 μ M Mn) flow
224 rate. Addition of a 0.46-mL aliquot of 0.65 M MnSO₄ stock solution to one of the 10-L reservoirs
225 imposed a 30- μ M Mn treatment. Two initial survey scans of 6 and 2 min identified the area for
226 detailed scans (Fig. 2c), the first of which started immediately thereafter (0 h). This and subsequent
227 detailed scans took *c.* 120 min to complete. There were six scans from 0-2, 6-8, 12-14, 18-20, 24-26,
228 and 48-50 h after first imposition of Mn treatments. The same procedures and scans of adjacent
229 unifoliate leaves followed with living plants in the second replicate. In the replicate reported here, the
230 detailed scan area was *c.* 120 mm², which included a leaf area of 55.2 and 56.4 mm² in the 0.2 and 30
231 μ M Mn treatments. The detailed scans had 4×4 μ m pixels and a velocity of 4 mm s⁻¹ resulting in a
232 pixel transit time of 1 ms. With a total photon flux of *c.* 2×10^9 photon s⁻¹ at an energy of 12.9 keV,
233 these scan parameters corresponded to *c.* 1.3×10^5 photon μ m⁻² for each scan (i.e. a total of 8.0×10^5
234 photon μ m⁻² for the six scans).

235 On completion of the scans, the CSIRO Dynamic Analysis method in GeoPIXE provided
236 quantitative, true-element images of X-ray fluorescence spectra (Ryan & Jamieson, 1993; Ryan,
237 2000) as outlined at <http://www.nmp.csiro.au/dynamic.html>. The survey scans required correction for
238 variation in leaf thickness arising from the major leaf veins by normalizing to Compton scatter.
239 Sections of leaves for detailed scans had only a few minor veins (Fig. 2c) that did not interfere greatly

240 with determination of the two-dimensional areal concentrations of elements and their distributions
241 (Kopittke *et al.*, 2011).

242 GeoPIXE provided initial quantitative analysis of Mn concentration in 2.6×0.08 mm
243 transects of detailed scans across the leaf at 30 μ M Mn from 0 to 48 h that involved 650 individual
244 pixels in the horizontal direction \times the mean of 20 pixels in the vertical direction. This was followed
245 by determining Mn in the high-resolution image area of 2.6×0.6 mm (i.e. values of individual $650 \times$
246 150 pixels). Further analysis using GeoPIXE and ImageJ 1.48v (Schneider *et al.*, 2012) extended the
247 two-dimension μ -XRF scans to a three-dimensional geometry of Mn distribution and concentration.
248 The number and localized areas of Mn accumulation and the distributions of K, Ca, Fe, Cu, and Zn at
249 0 and 48 h in the two Mn treatments were determined also.

250

251 **Results**

252

253 **Potential X-ray damage to living unifoliate leaves**

254

255 The Australian Synchrotron XFM beamline Maia detector system with fast data acquisition has the
256 advantage of rapid pixel transit times (Paterson *et al.*, 2011) but sequential *in situ* μ -XRF analyses of
257 hydrated leaf tissues may still result in radiation damage and tissue dehydration as shown in micro-
258 tomography of a cowpea root (Lombi *et al.*, 2011a). This was evident also in an unpublished study
259 using X-ray absorption near edge structure (XANES) imaging of a 4.0×2.5 mm section of a soybean
260 leaf at high Mn with repeated scans of the same area at increasing energy. Compared to the rest of the
261 leaf, the rectangular scanned area was mildly chlorotic suggestive of radiation damage (Fig. S1a).
262 Furthermore, there were changes in the distribution of Ca (Fig. S1b) and dehydration damage evident
263 in Compton scatter (Fig. S1c) though not in Mn distribution (data not presented). Although mapping
264 was conducted on-the-fly in the horizontal direction with a dwell of 1 ms per virtual 0.1-mm step,
265 damage occurred in a previous study at ends of the horizontal scan lines because of the increased
266 dwell of discrete steps in the vertical direction. In contrast to the effects observed in this previous
267 XANES imaging study, the preliminary experiment in the present study produced no evidence of
268 radiation damage or dehydration to a cowpea leaf after scanning for *c.* 2 h (Fig. 1). This was attributed
269 to the newly-implemented Rascan system which markedly reduced overheads, and hence reduced
270 dwell at the end of the horizontal lines during the vertical move to the next line. We therefore
271 concluded that rapid scanning prevented leaf damage suggesting that experimental artifacts would not
272 arise with time-resolved μ -XRF scans of living leaf tissues.

273

274 **Changes in elemental distribution and concentration**

275

276 There were no visible symptoms of Mn toxicity on leaves of plants grown for 7 d with the basal 0.2
277 μM Mn in solution (Fig. 1a) but there were a few localized spots of Mn accumulation visible in the μ -
278 XRF scans of the detached unifoliolate leaf during the preliminary experiment (Fig. 1b,c). This was
279 evident also at 0 h in both living cowpea unifoliolate leaves (Fig. 3) but it was only after 2 d at 30 μM
280 Mn that dark spots indicative of Mn accumulation were visible (Fig. 2c).

281 Visual assessment of the detailed μ -XRF scans (Fig. 3) indicated a slight increase over time in
282 the number of high-Mn spots at 0.2 μM Mn, but this increase was considerably lower than that with
283 30 μM Mn in solution. Given that each detailed scan was *c.* 8.5 megapixels, we selected a small area
284 of the image of 1.56 mm^2 ($2.6 \times 0.6 \text{ mm}$) to examine changes in elemental distribution in the 30- μM
285 Mn treatment over the 48-h experimental period. At the start of the experiment, high Mn spots were
286 visible to the left of the image, the largest being *c.* $240 \times 130 \mu\text{m}$ in size (Fig. 4). Elsewhere, Mn was
287 minimally above background. There was little change in Mn distribution after 6 h at 30 μM Mn, with
288 some new high Mn spots evident after 12 h and especially from 18 to 48 h. Transects across the
289 images from 0 to 48 h (Fig. 4) showed no visible increase in the number or concentration of high Mn
290 spots at 6 h, a few instances where new high Mn spots were visible at 12 h. It was only from 18 to 48
291 h, however, that there were clear increases in spot numbers and in their Mn concentration.

292 As demonstrated by Scheckel *et al.* (2004), ImageJ analysis of the high-resolution data at 30
293 μM Mn (Fig. 4) extended the two-dimensional μ -XRF scans to a three-dimensional geometry
294 providing visual images of both Mn distribution and concentration over the 48-h experimental period
295 (Fig. 5). As with the two-dimensional images (Figs 3, 4), there were a few spots of high Mn at the
296 start of the experiment with no discernable increase at 6 h. It appeared that the number and
297 concentration of Mn in these spots started to increase at 12 h followed by a further increase at 18 h
298 and marked increases at 24 h and 48 h.

299 Using the detailed scan areas of 55.2 and 56.4 mm^2 at 0.2 and 30 μM Mn (Fig. 3), we used
300 ImageJ to calculate the number of localized Mn spots at 0 h was 3.6 and 12.1 mm^{-2} in the two leaves
301 to be subjected to the 0.2 and 30 μM Mn treatments (Fig. 6a). The number of high-Mn spots appeared
302 unchanged over the first 6 h in both treatments. There was a slight increase over 48 h of 4 mm^{-2} at 0.2
303 μM Mn compared to the large increase of 30 mm^{-2} at 30 μM Mn. The corresponding increases in the
304 total area of localized high-Mn spots were < 0.001 and 0.04 $\text{mm}^2 \text{mm}^{-2}$ (Fig. 6b). Further analyses
305 using ImageJ determined that most of the initial high Mn spots were $< 320 \mu\text{m}^2$ in size (Fig. S2),
306 largely remaining so over 48 h at 0.2 μM Mn. This contrasted to the changes in spot size in the 30
307 μM -Mn treatment in which the percentage of spots $< 64 \mu\text{m}^2$ decreased over 48 h. Interestingly, the
308 percentage of slightly larger spots of 64 to $< 320 \mu\text{m}$ increased and then decreased and there was a
309 concomitant increase in large spots at 48 h.

310 With the μ -XRF scans providing quantitative, true-elemental data (Ryan & Jamieson, 1993;
311 Ryan, 2000), GeoPIXE analysis of the detailed μ -XRF scan of leaf sections at 48 h (Fig. 3)
312 determined mean values of 26 and 56 $\text{mg Mn kg}^{-1} \text{ FM}$ at 0.2 and 30 μM Mn. Analysis of the six

313 transects resulted in a calculated mean Mn concentration that increased from 35 to 61 mg kg⁻¹ FM
314 over 48 h exposure to 30 μM Mn (Table S1). However, these transects indicated that the background
315 Mn concentration was < 100 mg kg⁻¹ FM other than in the relatively few instances in which the Mn
316 concentration approached or exceeded 1,000 mg kg⁻¹ FM. Separating the data into two classes, above
317 and below an estimated background value of 60 mg kg⁻¹ FM, permitted further examination of leaf
318 Mn status. Pixel clusters with values < 60 mg Mn kg⁻¹ FM had a mean concentration of 24 mg Mn kg⁻¹
319 FM over 48 h, markedly lower than in those with values > 60 mg kg⁻¹ FM that increased from 200 to
320 420 mg Mn kg⁻¹ over 48 h (Table S1). Data from the 2.6 × 0.6 mm area used also to determine leaf
321 Mn concentration increased from a mean of 69 to 170 mg kg⁻¹ FM over 48 h (Table S1). These
322 estimates differed somewhat from the the bulk Mn concentration in entire unifoliolate leaves 48 h after
323 imposing the high Mn treatment of 11 ± 1 and 47 ± 14 mg kg⁻¹ FM at 0.2 and 30 μM Mn.
324 (Corresponding values were 80 ± 6 and 360 ± 110 mg kg⁻¹ DM.)

325 Finally, we utilized the μ-XRF analyses at 0 and 48 h to generate images for multiple
326 elements within the energy range of the beamline. In this exercise, the incident X-rays of 12.9 keV
327 and the Maia detector permitted investigation of the distributions and concentrations of elements
328 between P and Zn. (Selection of a higher incident energy would also permit analyses of heavier
329 elements.) The present study permitted investigation of six elements, K, Ca, Mn, Fe, Cu, and Zn, in
330 unifoliolate leaves that were above background concentrations (Fig. S3). At 0 h, there was relatively
331 even distribution of K and Ca across the leaves of plants at 0.2 μM Mn, as was that of Cu though at a
332 concentration close to the detection limit. In contrast, Mn and Fe accumulated in localized areas
333 across the leaf, but these elements were not co-located. Localized areas of high Zn were present in and
334 adjacent to the veins. The distributions of these elements were similar 48 h later at 0.2 μM Mn but the
335 distribution of Mn differed between the 0.2 and 30 μM Mn treatments as is evident in Fig. 3.

336

337 Discussion

338

339 The analysis of fresh tissues exacerbates the many challenges in μ-XRF scanning of low metal and
340 metalloid concentrations in biological tissues (Lombi *et al.*, 2011a). These challenges arise from
341 tissue hydration (often > 85 %) and the generally low concentrations of trace elements in tissues that
342 result in the consequent long transit times required for analysis. A high (long) dwell increases the
343 likelihood of radiation damage and tissue dehydration, thereby resulting in experimental artifacts that
344 affect element distribution (Lombi *et al.*, 2011a). The benchtop (i.e. non-synchrotron based) μ-XRF
345 method developed by Fittschen *et al.* (2017) ensured high sensitivity and low detection limits but
346 required dwells of 1 s per 40 × 40 μm pixel that resulted in substantial radiation damage to a scanned
347 *Arabidopsis thaliana* leaf. Scheckel *et al.* (2004) also noted that μ-XRF analysis using a 1-s dwell of a
348 6-μm pixel damaged leaves of living *Iberis intermedia* plants. As with these studies, our previous
349 unpublished work showed radiation damage and leaf dehydration was evident in a soybean leaf

350 subjected to multiple scanning (Fig. S1). Recent years, however, have seen major improvements in
351 overcoming these problems in synchrotron-based studies. This has been important in the study of
352 fresh, hydrated root (Kopittke *et al.*, 2011) and leaf tissues (Blamey *et al.*, 2015). Besides the high
353 spatial resolution of 0.1 to 0.2 μm at the Australian Synchrotron XFM beamline (Paterson *et al.*,
354 2011), there are inherent advantages of the Maia detector and Rascan in decreasing dwell. This was
355 evident in the preliminary experiment of the present study in which there was no visible X-ray
356 damage to a unifoliate cowpea leaf after two survey scans and four detailed scans with a combined
357 period of *c.* 2 h (Fig. 1). The recently updated raster scanning adds further advantages by decreasing
358 the damage to sensitive plant tissues.

359 Progress in μ -XRF analysis of hydrated plant tissues has been extended to leaf tissues of
360 living plants. For example, by growing the hyperaccumulator *I. intermedia* plants at elevated TI in
361 soil, Scheckel *et al.* (2004) determined that TI accumulated mostly in the vascular tissues. Fittschen *et*
362 *al.* (2017) constructed a benchtop μ -XRF unit to examine differences in the distributions of a number
363 of nutrients in the vascular system, mesophyll, and trichomes of leaves of living *A. thaliana* plants.
364 These studies, however, did not investigate time-resolved changes in elemental distribution and
365 concentration and we were not able to find instances in the literature of sequential μ -XRF analysis of
366 living plant tissues.

367 In the present study, μ -XRF detailed scans using a pixel size of $4 \times 4 \mu\text{m}$ enabled production
368 of high-quality images that permitted direct visual comparisons between the effects of 0.2 and 30 μM
369 Mn (Fig. 3) and enabled high resolution comparisons of Mn accumulation of 30 μM Mn over 48 h
370 (Fig. 4). A pixel size of $1 \times 1 \mu\text{m}$ allows even better resolution where appropriate (Blamey *et al.*,
371 2015). As demonstrated by Scheckel *et al.* (2004) and in the present study (Fig. 5), three-dimensional
372 representations of the two-dimensional scans provide further visualization of elemental distribution
373 and concentration.

374 Until recently, quantitative elemental analyses have focused on bulk tissues, from whole
375 plants to separate analyses of roots, shoots, stems, and leaves (Salt *et al.*, 2008) but technological
376 developments in synchrotron-based μ -XRF, amongst other techniques, provide greater spatial
377 resolution of the ionome (Punshon *et al.*, 2009; van der Ent *et al.*, 2017). However, van der Ent *et al.*
378 (2017) urged caution in the use of μ -XRF in foliar studies using living plants because measurements
379 arise from different depths, from different cell types (e.g., epidermis, palisade, mesophyll, and
380 vasculature), and from continued plant metabolism. The first two of these potential difficulties may be
381 addressed by a combination of analytical techniques as shown by Blamey *et al.* (2017) who used
382 NanoSIMS to confirm the suspected accumulation of Mn in the apoplast using μ -XRF by analysis.
383 The present study has also shown that accommodation of continued plant metabolism is possible,
384 albeit in only one instance of Mn accumulation. High Mn accumulation in discreet locations is of
385 additional benefit by overcoming the overall low concentrations of many trace elements.

386 It has been recognized for many years that symptoms of Mn toxicity precede a decrease in
387 plant growth (Foy *et al.*, 1978; Weil *et al.*, 1997), information extended by Fernando *et al.* (2016)
388 with Mn accumulation in leaves of wheat (*Triticum aestivum*) plants well before the appearance of
389 visible symptoms. This was evident in leaves of cowpea exposed to a non-toxic concentration of 0.2
390 μM Mn (Figs 1, 3, 4, 5). Localized spots of high Mn preceded visible symptoms associated with Mn
391 toxicity in the present study also with new high Mn spots first visible after 12 h growth at 30 μM Mn
392 (Figs 4, 5) but visible dark spots appeared only after 48 h (Fig. 2c). However, the mechanism is
393 unknown whereby high Mn accumulates in specific localized areas not visibly associated with leaf
394 anatomy (e.g., close to or distant from veins). There is similar uncertainty as to why an overall
395 increase in Mn in leaf tissues at 30 μM Mn (Figs 4 and 5) results in localized increases in Mn but no
396 general increase in background Mn concentration over time.

397 From an ionomics viewpoint (Salt *et al.*, 2008), the present study addressed various
398 microscopic measures of Mn concentration in leaf tissues based on the true-elemental data of the μ -
399 XRF scans. After 48 h at 0.2 μM Mn, these analyses ranged from 24 to 35 mg Mn kg^{-1} FM compared
400 to the unifoliolate leaf bulk analysis of 11 mg Mn kg^{-1} FM. The corresponding comparison was 56 to
401 169 mg kg^{-1} versus a bulk leaf tissue concentration of 47 mg Mn kg^{-1} FM at 30 μM Mn. While of the
402 same order of magnitude, these findings suggest that further research is required in the sampling for
403 quantitative determination of elemental concentrations in leaf tissues. Importantly, the multi-element
404 analyses undertaken in the present study would provide important information on interactions
405 between the various elements. An example relevant to the present study might use detailed μ -XRF
406 studies to examine the kinetics of changes in Mn distribution (Figs 4, 5) with those of Ca (Fig. S3)
407 given the role of Ca in callose formation associated with Mn toxicity (Wissemeier & Horst, 1987).
408 Additional studies may also provide critical information as to the underlying mechanisms whereby
409 Mn is toxic by determining changes in Ca and Mn accumulation in the apoplast and by determining
410 how Mn accumulates along with Ca in vacuoles of some plant species but not in others. Finally, there
411 is particular promise in studies such as that by Takahashi *et al.* (2009) in combining information on
412 the activities of metal transporter genes with multi-element μ -XRF analysis of changes in the
413 distribution of Fe, Mn, Cu, and Zn in germinating rice (*Oryza sativa*) seeds.

414

415 **Conclusion**

416

417 Development of a synchrotron-based method has shown the feasibility of using μ -XRF analysis to
418 determine the distribution and concentration of Mn in living unifoliolate leaves of cowpea exposed to
419 0.2 and 30 μM Mn in solution culture. This method may be adapted to examine the accumulation and
420 distribution of other elements and plant species over a range in exposure times. Besides investigations
421 of elemental toxicities, other examples may include determining the dynamics of nutrients upon

422 addition to a nutrient-deficient plant, the effects of hypoxia on nutrient status, and establishing the
423 relationship between transpiration and nutrient accumulation in leaf tissues.

424 The results and implications of the present study advance the value of ionomics, the inorganic
425 component of the metabolome, through quantifying changes in the microscopic distribution and
426 concentration of elements *in vivo* (Salt *et al.*, 2008). Though focusing the present study on the kinetics
427 of Mn accumulation in cowpea unifoliolate leaves, μ -XRF analyses may also provide multi-element
428 information in plant tissues, meeting an aim of ionomics to define the functional state of an organism
429 driven by genetic, developmental, biotic, or abiotic influences.

430

431

432 **Acknowledgements**

433

434 F.P.C.B. acknowledges assistance from the Australian Government Research Training Program and
435 P.M.K. acknowledges receipt of an Australian Research Council (ARC) Future Fellowship
436 (FT120100277). This research was undertaken on the XFM beamline (Project AS153/XFM/11040) at
437 the Australian Synchrotron, part of the Australian Nuclear Science and Technology Organization
438 (ANSTO). We thank Dr Chris Ryan (CSIRO), Dr Martin de Jonge, and Dr Daryl Howard (Australian
439 Synchrotron) for assistance with synchrotron-based techniques.

440

441 **Author contributions**

442

443 F.P.C.B. conceived the research program that was developed in collaboration with D.J.P., A.W.,
444 N.W.M., and P.M.K.; A.W. and N.A. developed the requisite technology; F.P.C.B., M.C., and C.T.
445 conducted the plant growth experiments; F.P.C.B., D.J.P., B.A.M., M.C., and P.M.K. conducted the
446 μ -XRF analyses at the Australian Synchrotron; F.P.C.B and P.M.K. analyzed the data; and F.P.C.B.,
447 D.J.P, and P.M.K. wrote the first draft of the article to which all authors contributed.

448

449 **References**

- 450 **Babourina O, Rengel Z. 2009.** Uptake of aluminium into *Arabidopsis* root cells measured by
451 fluorescent lifetime imaging. *Annals of Botany* **104**: 189-195.
- 452 **Blamey FPC, Hernandez-Soriano MC, Cheng M, Tang C, Paterson DJ, Lombi E, Wang WH,**
453 **Scheckel KG, Kopittke PM. 2015.** Synchrotron-based techniques shed light on mechanisms
454 of plant sensitivity and tolerance to high manganese in the root environment. *Plant*
455 *Physiology* **169**: 2006-2020.
- 456 **Blamey FPC, McKenna BA, Li C, Cheng M, Tang C, Jiang H, Howard DL, Paterson DJ,**
457 **Kappen P, Wang P, et al. 2017.** Manganese distribution and speciation help to explain the
458 effects of silicate and phosphate on manganese toxicity in four crop species. *New Phytologist*.
459 doi: 10.1111/nph.14878.
- 460 **Bravo P, Uribe EG. 1981.** Temperature dependence of the concentration kinetics of absorption of
461 phosphate and potassium in corn roots. *Plant Physiology* **67**: 815-819.
- 462 **Conn S, Gilliam M. 2010.** Comparative physiology of elemental distributions in plants. *Annals of*
463 *Botany* **105**: 1081-1102.
- 464 **Cosio C, DeSantis L, Frey B, Diallo S, Keller C. 2005.** Distribution of cadmium in leaves of *Thlaspi*
465 *caerulescens*. *Journal of Experimental Botany* **56**: 765-775.
- 466 **Danilatos GD. 1981.** The examination of fresh or living plant material in an environmental scanning
467 electron microscope. *Journal of Microscopy* **121**: 235-238.
- 468 **Fernando DR, Moroni SJ, Scott BJ, Conyers MK, Lynch JP, Marshall AT. 2016.** Temperature
469 and light drive manganese accumulation and stress in crops across three major plant families.
470 *Environmental and Experimental Botany* **132**: 66-79.
- 471 **Fittschen UEA, Kunz HH, Hohner R, Tyssebotn IMB, Fittschen A. 2017.** A new micro X-ray
472 fluorescence spectrometer for *in vivo* elemental analysis in plants. *X-Ray Spectrometry* **46**:
473 374-381.
- 474 **Foy CD, Chaney RL, White MC. 1978.** The physiology of metal toxicity in plants. *Annual Review*
475 *of Plant Physiology* **29**: 511-566.
- 476 **Heenan DP, Carter OG. 1976.** Tolerance of soybean cultivars to manganese toxicity. *Crop Science*
477 **16**: 389-391.
- 478 **Hevesy G. 1923.** The absorption and translocation of lead by plants. A contribution to the application
479 of the method of radioactive indicators in the investigation of the change of substance in
480 plants. *Biochemical Journal* **17**: 439-445.
- 481 **Horst WJ. 1983.** Factors responsible for genotypic manganese tolerance in cowpea (*Vigna*
482 *unguiculata*). *Plant and Soil* **72**: 213-218.
- 483 **Jahnke S, Menzel MI, van Dusschoten D, Roeb GW, Buhler J, Minwuyelet S, Blumler P,**
484 **Temperton VM, Hombach T, Streun M, et al. 2009.** Combined MRI-PET dissects dynamic
485 changes in plant structures and functions. *Plant Journal* **59**: 634-644.

- 486 **Kopittke PM, Blamey FPC, Asher CJ, Menzies NW. 2010.** Trace metal phytotoxicity in solution
487 culture: A review. *Journal of Experimental Botany* **61**: 945-954.
- 488 **Kopittke PM, Lombi E, McKenna BA, Wang P, Donner E, Webb RI, Blamey FPC, de Jonge**
489 **MD, Paterson D, Howard DL, et al. 2013.** Distribution and speciation of Mn in hydrated
490 roots of cowpea at levels inhibiting root growth. *Physiologia Plantarum* **147**: 453-464.
- 491 **Kopittke PM, Menzies NW, de Jonge MD, McKenna BA, Donner E, Webb RI, Paterson DJ,**
492 **Howard DL, Ryan CG, Glover CJ, et al. 2011.** In situ distribution and speciation of toxic
493 copper, nickel, and zinc in hydrated roots of cowpea. *Plant Physiology* **156**: 663-673.
- 494 **Kopittke PM, Moore KL, Lombi E, Gianoncelli A, Ferguson BJ, Blamey FPC, Menzies NW,**
495 **Nicholson TM, McKenna BA, Wang P, et al. 2015.** Identification of the primary lesion of
496 toxic aluminum in plant roots. *Plant Physiology* **167**: 1402-1411.
- 497 **Lombi E, de Jonge MD, Donner E, Kopittke PM, Howard DL, Kirkham R, Ryan CG, Paterson**
498 **D. 2011a.** Fast X-ray fluorescence microtomography of hydrated biological samples. *PLoS*
499 *ONE* **6**: 1-5.
- 500 **Lombi E, Smith E, Hansen TH, Paterson D, de Jonge MD, Howard DL, Persson DP, Husted S,**
501 **Ryan C, Schjoerring JK. 2011b.** Megapixel imaging of (micro)nutrients in mature barley
502 grains. *Journal of Experimental Botany* **62**: 273-282.
- 503 **Lombi E, Susini J. 2009.** Synchrotron-based techniques for plant and soil science: opportunities,
504 challenges and future perspectives. *Plant and Soil* **320**: 1-35.
- 505 **McGregor JE, Donald AM 2010.** The application of ESEM to biological samples. In: Baker RT ed.
506 *Electron Microscopy and Analysis Group Conference 2009*, 012021.
- 507 **McNear DH, Peltier E, Everhart J, Chaney RL, Sutton S, Newville M, Rivers M, Sparks DL.**
508 **2005.** Application of quantitative fluorescence and absorption-edge computed
509 microtomography to image metal compartmentalization in *Alyssum murale*. *Environmental*
510 *Science & Technology* **39**: 2210-2218.
- 511 **McNear DHJ, Küpper JV. 2014.** Mechanisms of trichome-specific Mn accumulation and toxicity in
512 the Ni hyperaccumulator *Alyssum murale*. *Plant and Soil* **377**: 407-422.
- 513 **Moore KL, Chen Y, van de Meene AML, Hughes L, Liu WJ, Geraki T, Mosselmans F,**
514 **McGrath SP, Grovenor C, Zhao FJ. 2014.** Combined NanoSIMS and synchrotron X-ray
515 fluorescence reveal distinct cellular and subcellular distribution patterns of trace elements in
516 rice tissues. *New Phytologist* **201**: 104-115.
- 517 **Paterson DJ, de Jonge MD, McKinlay WLJ, Starritt A, Kusel M, Ryan CG, Kirkham R,**
518 **Moorhead G, Siddons DP. 2011.** The X-ray fluorescence microscopy beamline at the
519 Australian synchrotron. *AIP Conference Proceedings* **1365**: 219-222.
- 520 **Punshon T, Guerinot ML, Lanzirotti A. 2009.** Using synchrotron X-ray fluorescence microprobes
521 in the study of metal homeostasis in plants. *Annals of Botany* **103**: 665-672.

- 522 **Ryan CG. 2000.** Quantitative trace element imaging using PIXE and the nuclear microprobe.
523 *International Journal of Imaging Systems and Technology* **11**: 219-230.
- 524 **Ryan CG, Jamieson DN. 1993.** Dynamic analysis: on-line quantitative PIXE microanalysis and its
525 use in overlap-resolved elemental mapping. *Nuclear Instruments & Methods in Physics*
526 *Research Section B-Beam Interactions with Materials and Atoms* **77**: 203-214.
- 527 **Salt DE, Baxter I, Lahner B. 2008.** Ionomics and the study of the plant ionome. *Annual Review of*
528 *Plant Biology* **59**: 709-733.
- 529 **Scheckel KG, Lombi E, Rock SA, McLaughlin MJ. 2004.** In vivo synchrotron study of thallium
530 speciation and compartmentation in *Iberis intermedia*. *Environmental Science & Technology*
531 **38**: 5095-5100.
- 532 **Schneider CA, Rasband WS, Eliceiri KW. 2012.** NIH Image to ImageJ: 25 years of image analysis.
533 *Nature Methods* **9**: 671-675.
- 534 **Solon EG, Schweitzer A, Stoekli M, Prideaux B. 2010.** Autoradiography, MALDI-MS, and SIMS-
535 MS imaging in pharmaceutical discovery and development. *The AAPS Journal* **12**: 11-26.
- 536 **Sugita R, Kobayashi NI, Hirose A, Saito T, Iwata R, Tanoi K, Nakanishi TM. 2016.** Visualization
537 of uptake of mineral elements and the dynamics of photosynthates in Arabidopsis by a newly
538 developed real-time radioisotope imaging system (RRIS). *Plant and Cell Physiology* **57**: 743-
539 753.
- 540 **Takahashi M, Nozoye T, Kitajima N, Fukuda N, Hokura A, Terada Y, Nakai I, Ishimaru Y,**
541 **Kobayashi T, Nakanishi H, et al. 2009.** In vivo analysis of metal distribution and expression
542 of metal transporters in rice seed during germination process by microarray and X-ray
543 Fluorescence Imaging of Fe, Zn, Mn, and Cu. *Plant and Soil* **325**: 39-51.
- 544 **Tsukamoto T, Nakanishi H, Kiyomiya S, Watanabe S, Matsubishi S, Nishizawa NK, Mori S.**
545 **2006.** ⁵²Mn translocation in barley monitored using a positron-emitting tracer imaging system.
546 *Soil Science and Plant Nutrition* **52**: 717-725.
- 547 **van der Ent A, Przybyłowicz WJ, de Jonge MD, Harris HH, Ryan CG, Tylko G, Paterson DJ,**
548 **Barnabas AD, Kopittke PM, Mesjasz-Przybyłowicz J. 2017.** X-ray elemental mapping
549 techniques for elucidating the ecophysiology of hyperaccumulator plants. *New Phytologist*.
550 doi: 10.1111/nph.14810.
- 551 **Walczyński P, Wagner E, Albrechtová JTP. 2000.** Use of co-loaded Fluo-3 and Fura Red
552 fluorescent indicators for studying the cytosolic Ca²⁺ concentrations distribution in living
553 plant tissue. *Cell Calcium* **28**: 23-32.
- 554 **Weil RR, Foy CD, Coradetti CA. 1997.** Influence of soil moisture regimes on subsequent soil
555 manganese availability and toxicity in two cotton genotypes. *Agronomy Journal* **89**: 1-8.
- 556 **Wissemeyer AH, Horst WJ. 1987.** Callose deposition in leaves of cowpea (*Vigna unguiculata* (L.)
557 Walp.) as a sensitive response to high Mn supply. *Plant and Soil* **102**: 283-286.
- 558

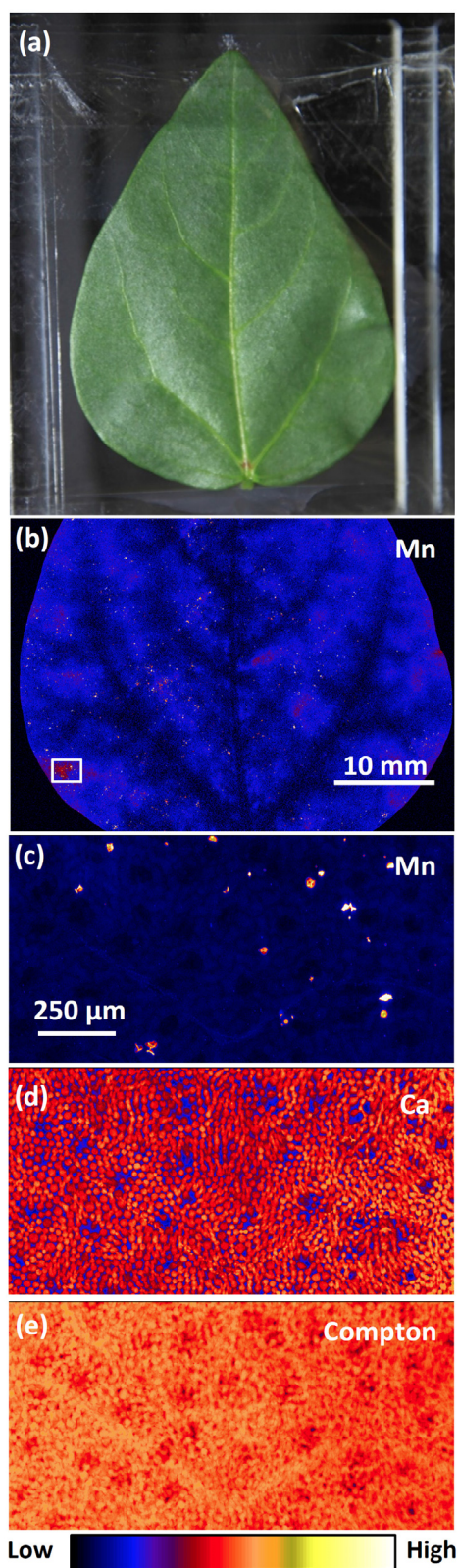


Fig. 1. Images of a detached unifoliate leaf of cowpea grown for 7 d at 0.2 μ M Mn after conducting a survey scan and three detailed scans. (a) Optical image of a leaf mounted between Ultralene® films. (b) Survey μ -XRF scan of Mn distribution, the white box showing the area of subsequent detailed scans. (c,d) Detailed μ -XRF scan showing the distributions of Mn and Ca. (e) Detailed Compton scatter.

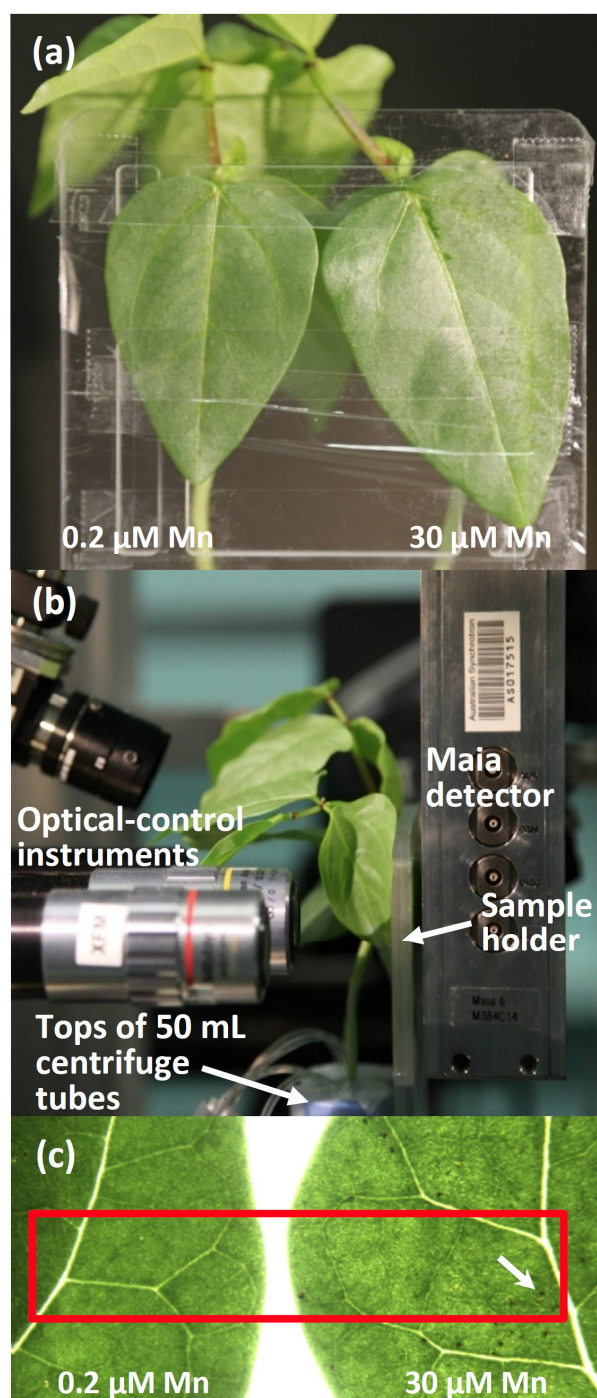


Fig. 2. Optical images of cowpea unifoliolate leaf arrangement in the sample holder. (a) Leaves of two plants grown at 0.2 and 30 μM Mn between Ultralene[®] films in the sample holder. (b) Arrangement of living plants mounted in the X-ray beam. (c) Micrograph of unifoliolate leaves after the detailed $\mu\text{-XRF}$ scan at 48 h, the red box showing the area of sequential detailed scans and the white arrow a visible dark spot of Mn accumulation at 30 μM Mn.

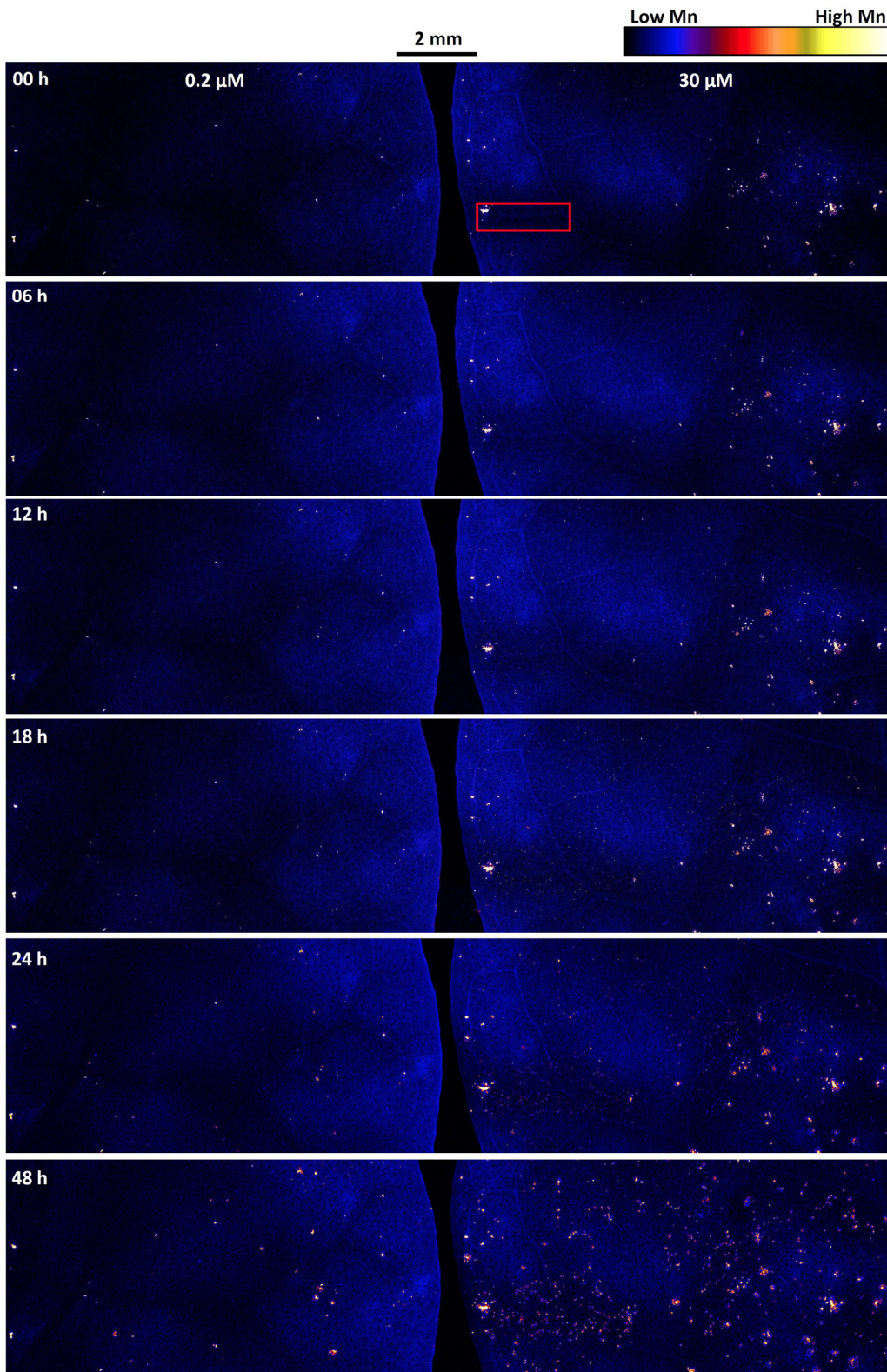


Fig. 3. Detailed μ -XRF scans of Mn distribution in unifoliolate leaves of cowpea from 0 to 48 h after initial exposure to 30 μ M Mn in solution culture. The red box at 0 h shows the area analyzed at high resolution for the distribution of Mn (Fig. 4), for three-dimensional representation of Mn distribution and concentration (Fig. 5), and for ImageJ and GeoPIXE analyses (Fig. 6).

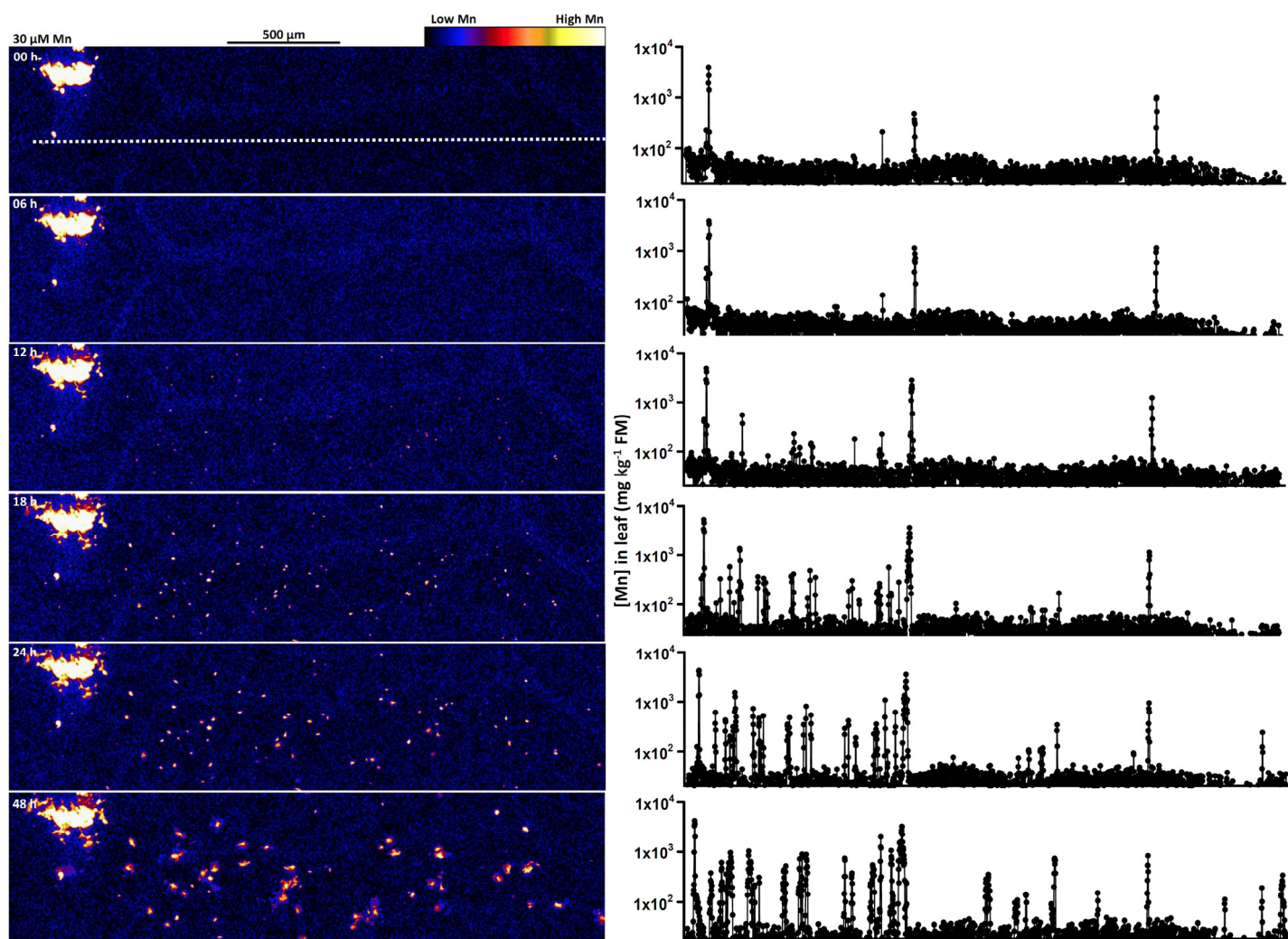


Fig. 4. High-resolution μ -XRF scans and transects of Mn distribution and concentration (log₁₀ scale) from 0 to 48 h after initial exposure to 30 μ M Mn in a 2.6 mm \times 0.6 mm section of a cowpea unifoliolate leaf (Fig. 3). The horizontal dotted line at 0 h identifies the position of transects along which the concentration of Mn was determined.

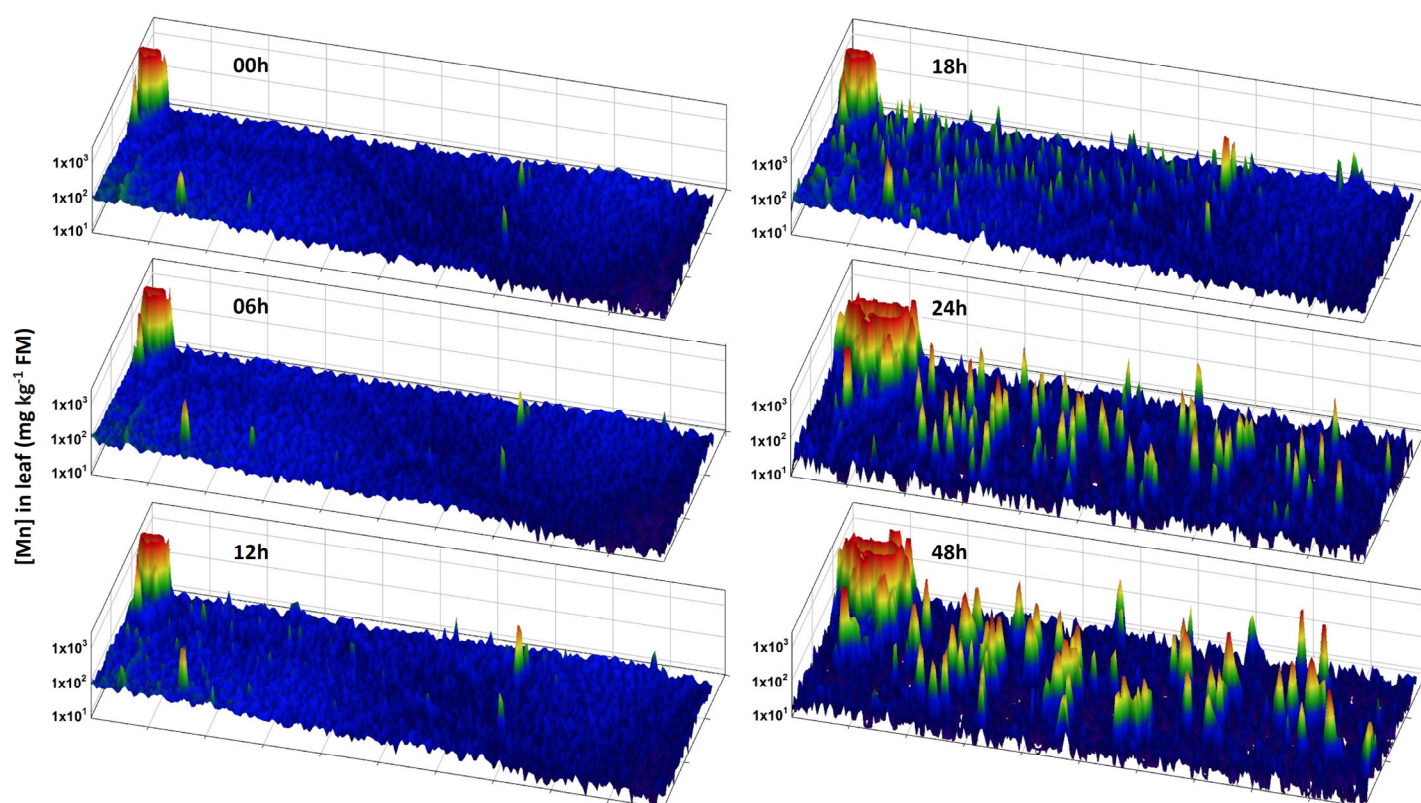


Fig. 5. Three-dimensional representation of Mn distribution and concentration in unifoliolate leaf sections of cowpea from 0 to 48 h after initial exposure to 30 μ M Mn. The scanned area is 2.6 mm \times 0.6 mm as shown by the red box in Fig. 3 and the high-resolution μ -XRF images in Fig. 4. The Mn concentration in the large high-Mn spot (back left) exceeded 10,000 mg kg⁻¹ FM from 0 to 48 h but the scale of Mn in the unifoliolate leaf has been limited to 1,000 mg kg⁻¹ FM to show the change in high Mn spots that developed during the 48-h experimental period.

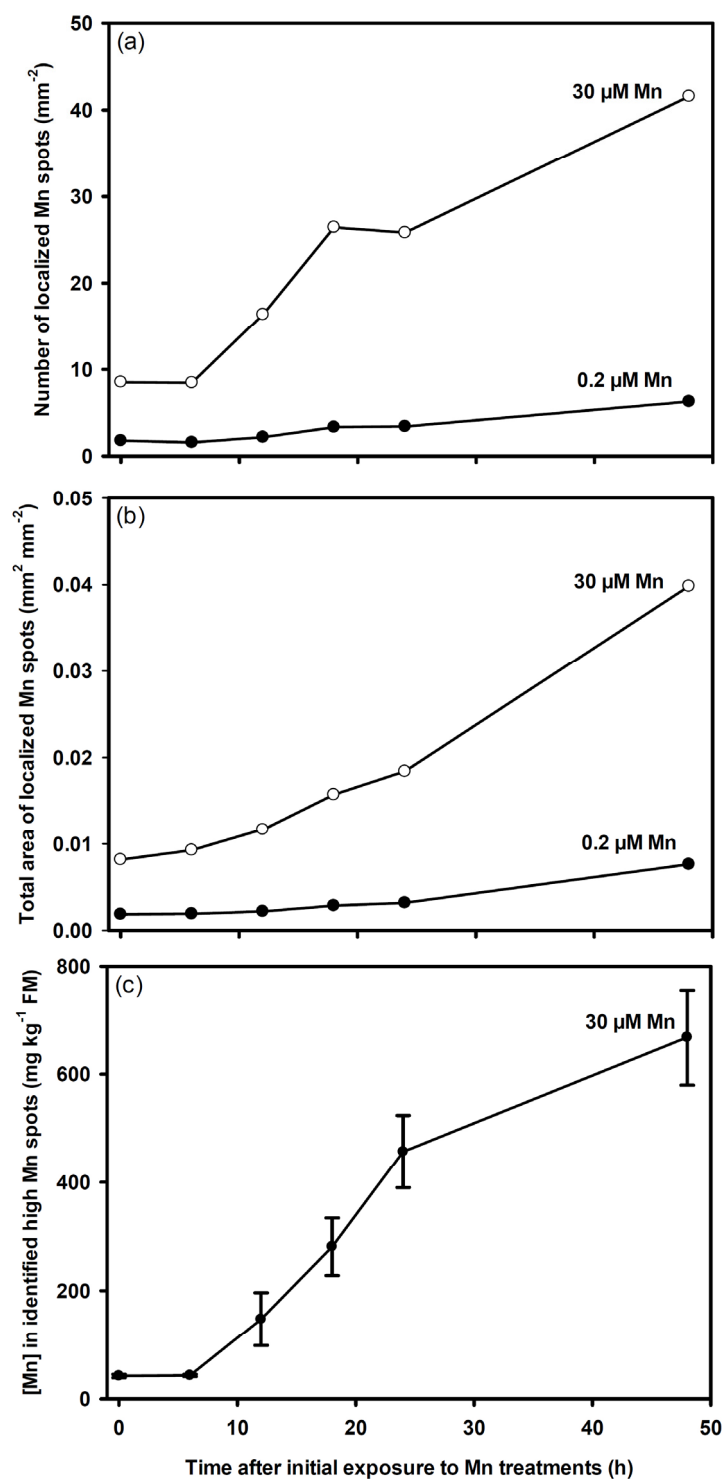


Fig. 6. Accumulation of Mn in unifoliolate leaf sections (Fig. 3) of cowpea from 0 to 48 h after initial exposure to 30 μM Mn in solution culture. (a,b) ImageJ determination of the number and area of localized spots of high Mn in detailed scans of leaf sections (Fig. 3). (c) GeoPIXE determination of the Mn concentration in identified high Mn spots (i.e. $> 60 \text{ mg kg}^{-1} \text{FM}$) over 48 h in transects of the section of a cowpea unifoliolate leaf at 30 μM Mn (Fig. 4).